

Article

Study on Performance Optimization of Water-Rich Grouting Materials Based on Response Surface Methodology

Xiaoping Li ¹, Guoping Han ¹, Yong Wang ¹, Jie Xu ¹, Jie Du ¹, Bo Yang ¹, Min Zhang ¹, Tao Li ¹ and Bo Li ^{2,*}

¹ Tunlan Mine, Shanxi Coking Coal Group Co., Ltd., Gujiao 030206, China; lixiaoping7526@163.com (X.L.); hanguoping0802@163.com (G.H.); wangyong202308@163.com (Y.W.); ky921899@126.com (J.X.); dujie20220502@163.com (J.D.); yangbo202308@163.com (B.Y.); chenycumt@sina.com (M.Z.); aqkygc@126.com (T.L.)

² School of Safety Science and Engineering, Henan Polytechnic University, Jiaozuo 454003, China

* Correspondence: anquanlibo@163.com

Abstract: The quality of borehole sealing is a key factor affecting the efficiency of gas production. A new water-rich grouting material (RW) with composite coagulant and other additives was prepared in this study to overcome the disadvantages of long setting time and low stone rate of traditional cement materials. When the coagulants A is 4 g and coagulants B is 2 g, the setting time of RW material was reduced by 60.85% and 50.62%, which significantly shortened the setting time of the RW material, respectively. Based on the orthogonal method, 29 groups of comparative experiments were designed to investigate the interaction mechanism between different additives on the performance index of RW, including setting time, water secretion rate, and compressive strength. Quadratic regression equations were fitted using the response surface method. All the correlation coefficients R^2 of each response model were greater than 0.97, R^2 and R^2_{adj} were less than 0.2 through variance analysis, indicating a high correlation between the actual and prediction results. The water–cement ratio had the most significant effect among all factors on setting time, water secretion rate, and compressive strength of the RW material. The scanning electron microscope (SEM) was used to compare the micromorphological characteristics of RW and conventional Portland cement material (PC). The results showed that the hydration products of RW were mostly smectite, calcium silicate hydrate gel, and calcium hydroxide, which interweaved with each other to form a network structure that was denser than the PC material. Furthermore, the interface bonding degree between RW and injected coal was tighter than that of PC, without obvious cracks at the slurry–coal interface. The results indicate that the addition of composite coagulant can significantly accelerate the hydration process of RW material and also enhance the interface strength of injected coal, which is conducive to improving the grouting quality and sealing effect of the extraction borehole.

Keywords: gas extraction; water-rich grouting materials; orthogonal experiment methodology; response surface methodology; scanning electron microscope



Citation: Li, X.; Han, G.; Wang, Y.; Xu, J.; Du, J.; Yang, B.; Zhang, M.; Li, T.; Li, B. Study on Performance Optimization of Water-Rich Grouting Materials Based on Response Surface Methodology. *Processes* **2023**, *11*, 2789. <https://doi.org/10.3390/pr11092789>

Academic Editor: Vladimir S. Arutyunov

Received: 13 August 2023

Revised: 10 September 2023

Accepted: 17 September 2023

Published: 19 September 2023



Copyright: © 2023 by the authors. Licensee MDPI, Basel, Switzerland. This article is an open access article distributed under the terms and conditions of the Creative Commons Attribution (CC BY) license (<https://creativecommons.org/licenses/by/4.0/>).

1. Introduction

Coalbed methane (CBM), a type of unconventional natural gas co-born with coal, has significant reserves in China and can reach up to $36.81 \times 10^{12} \text{ m}^3$ at a shallow depth of 2000 m, with recoverable resources of $10.87 \times 10^{12} \text{ m}^3$ (about 30%) and a large potential for development [1–3]. CBM is an efficient and clean energy source that brings considerable economic benefits, which is of great importance in alleviating the constricted natural gas supply [4]. However, the continuous development of deep CBM, the characteristics of high stress, and gas pressure are more likely to cause coal and gas outburst disasters. Wang et al. [5] developed a system for the in situ monitoring of spontaneous combustion gas emissions from fissure channels by considering spontaneous combustion gas, meteorological factors, and the thermal physical characteristics of fissures, and providing support for

taking corresponding fire extinguishing measures for the degree of coal fire re-ignition in coal fire areas. Bosikov et al. [6] developed a new modeling method for mine ventilation networks to reduce the cost of eliminating mine fires, in order to improve the reliability of mine gas mode control. Silva et al. [7] introduced the main technical differences of ICs in order to provide a type of guideline on the use of these reactive fire protections. This condition seriously limits the safe and efficient production of coal mines [8]. How to efficiently extract and utilize CBM is currently an urgent problem.

Pre-extraction through boreholes is a prominent technique for achieving efficient gas extraction from coal seams [9]. The deep coal seams in China are characterized by high geostress, high gas content, high gas stress, and low permeability, thus leading to a difficult extraction process, including borehole collapse, inadequate sealing of borehole plugging, and other phenomena [10,11]. Therefore, the selection of suitable grouting plugging materials is one of the key factors to improving gas extraction [12,13]. In this regard, related scholars have achieved many results in their research on the mechanism of grouting plugging. Wang et al. [14] studied the influence of sealing support force on the air leakage rate of boreholes, proposed the principle of active support grouting sealing, and analyzed the factors that affect the air leakage rate. Zhang et al. [15] systematically investigated the evolution law of permeability by establishing a two-media coupling model considering matrix shrinkage and effective stress. They found that the gas concentration increases with the increase in the seal length and pore diameter, and decreases with the increase in the negative pressure of pumping and coal permeability. Wang et al. [16] discussed the effects of extraction time, seal length, and air leakage rate on gas concentration by constructing a fluid–solid coupling model. Si et al. [17] developed a self-healing sealing material to reduce the impact of regenerated fractures on gas extraction efficiency, which can achieve self-healing of fractures. Xia et al. [18] systematically explored the effects of different seal lengths, leakage rates, and leakage crack widths on the concentration of gas discharged from the cracks by establishing a coupled model of coal seam deformation, coal seam gas flow and transport, and air flow in the coal seam. For cement additives, Chen et al. [19] synthesized a reactive halogen-free organic grouting reinforcement material with excellent thermal stability to address the problem of high halogen content in ordinary polyurethane grouting reinforcement materials, which causes catalyst poisoning and deactivation in coal chemical enterprises. Sun et al. [20] developed a new cement grouting materials and used scanning electron microscopy (SEM) to observe the product morphology under different sodium hydroxide dosages. Zhao et al. [21] analyzed the role of aluminate cement in the curing and expansion mechanism of the material by testing different aluminate cement dosages. Liu et al. [22] introduced 2-Acrylamido-2-methylpropanesulfonic acid combined with triethanolamine as an organic early strengthening component. They investigated the preparation and performance of the early strengthening agent through orthogonal tests and thermogravimetric analysis, X-ray diffraction analysis, and SEM. Qian et al. [23] conducted experiments on the water absorption performance of water absorbing resins in different slurry environments. They verified that using water-absorbing resins as the stopping grouting of boreholes grouting can significantly reduce the compressive strength of the cement in contact with it, and the influence range is about 100 mm. Guan et al. [24] developed an inorganic and organic composite grouting reinforcement material for deep soft rock based on prominent issues such as large deformation, crack closure, and permeability of surrounding rock in soft rock tunnels with a depth of one kilometer. The material exhibits “high early strength, high injectability, and high adhesion”.

For sealing the borehole using grouting, improving the performance of grouting materials is the key to improving the effectiveness of sealing. On the basis of previous research, this work formulates a water-rich grouting material (RW) with composite coagulants, analyzes the changes of setting time, water secretion rate, and compressive strength of RW by using the response surface method (RSM), and observes the microscopic microstructure characteristics of RW and Portland cement (PC). The microstructure of RW and injected coal is studied by using SEM, and the hydration process of slurry and hydration prod-

ucts is analyzed, thus providing a theoretical basis for improving the quality of grouting and sealing.

2. Materials Preparation and Test Methods

2.1. Raw Materials

RW is prepared by using ordinary PC as the base material, with compound component coagulant and a few additives. Its water–cement ratio can reach 1.0. The main mineral components of the base material are tricalcium silicate (C_3S), dicalcium silicate (C_2S), tricalcium chlorate (C_3A), tetracalcium aluminoferrite (C_4AF), and some free calcium oxide and magnesite. The mineral composition of coagulant A is mainly calcium sulfoaluminate (C_4A_3S'), C_2S , and so on. The main component of coagulant B is carbonate, and the main component of coagulant C is a complex of sulphate and calcium formate. The main component of the suspension is montmorillonite.

To understand the composition of hydration products in the preparation engineering of RW and PC materials, two sets of RW and PC materials were prepared. The phase differences between the two materials were compared through X-ray diffraction, in order to provide theoretical support for slurry improvement. The physical phase analysis of the mineral composition of RW and PC materials is shown in Figure 1. A certain amount of C_3S , C_2S , C_3A , C_4AF , and C_4A_3S' are present in the mineral composition of cement. C_3S can hydrate with C_2S to form C-S-H gels, C_3A will hydrate with C_4AF to form CH gels, and C_4A_3S' hydration can react rapidly with gypsum to form smack ettringite (AFt) in the early stages of hydration. The hydration of the mineral components to form calcium aluminate crystals of different amounts and morphology will result in different grout properties, which will affect the grouting and sealing performance.

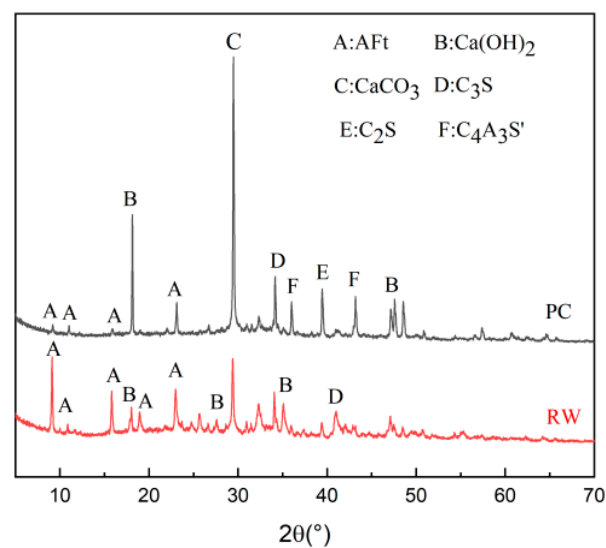


Figure 1. Physical composition analysis of basic materials.

2.2. Test Program

In the process of preparing grouting materials, a group of RW materials without the addition of coagulants was preferentially prepared and its slurry setting time was measured, which was found to be approximately 567 min, and the phenomenon of water secretion occurred. Therefore, a comparative experiment was carried out with the addition of three different coagulants to investigate the effect of the type and dosage of coagulants on the RW materials.

2.3. Test Methods

(1) Test for setting time

The time taken from the completion of the slurry preparation to the setting is known as the setting time. The slurry setting time was based on GB1346-89 “Test methods for water requirement of normal consistency, setting time and soundness of Portland cement”, which was applied using the ISO standard method of the Vickers apparatus [25].

(2) Test for water secretion rate

The water secretion rate was tested by first weighing the sample cylinder. Then, the mixed slurry was loaded into the sample cylinder and smoothed at the opening [26]. The outer surface and mouth of the specimen cylinder were wiped clean, and the total weight of the stirred slurry and the specimen cylinder were weighed. Afterward, the timer was started. Finally, the remaining weight of the slurry and sample cylinder was weighed at the end of water secretion. The rate of water secretion was calculated using Formula (1), and the water secretion rate is accurate to 0.01% [27].

$$c = \frac{a - b}{a} \times 100\% \quad (1)$$

where a is the full cylinder mass, g; b is the residual mass, g; and c is the water secretion rate, %.

(3) Test for compressive strength

The uniaxial compression test was conducted on the prepared standard specimens under standard preservation conditions using the RMT-150 rock mechanics test system manufactured by the Wuhan Institute of Geotechnics, Chinese Academy of Sciences [28,29]. The experimental equipment and procedure are shown in Figure 2. The maximum horizontal load of the test system was up to 500 kN, the maximum axial load was up to 1000 kN, the maximum peripheral pressure was 50 MPa, the maximum axial travel was 50 mm, the displacement was 5 mm, and the transverse displacement was 2.5 mm. This test adopts the displacement loading method, and the loading rate was 0.12 mm/min. We mixed cement, admixtures, and water in a water–cement ratio of 0.8(A), 1.0(B), and 1.2(C) to produce three sets of slurry. Once the mixture was uniformly mixed, we poured it into a mold with a diameter of 61.8 mm and a height of 20 mm. We smoothed the surface and allowed it to cure at room temperature for 24 h before removing it from the mold. Afterward, we cured it in a standard curing room for 28 days to test its compressive strength. The process is outlined in Figure 2.

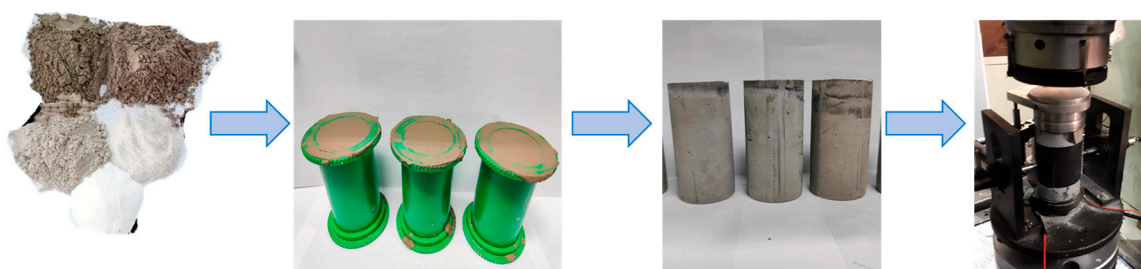


Figure 2. Flow chart of compressive strength experiment.

The compressive strength test results are shown in Figure 3, where A experiences shear failure. When the cylindrical specimen is subjected to pressure, shear failure may occur at the center of the specimen. This type of failure is more common when the material has high shear strength. B undergoes crush. When the pressure on the sample exceeds its compressive capacity, the sample may experience crush, which is more common when the compressive strength of the material is low. C exhibits delamination failure, and the surface of the sample exhibits layered delamination or cracks.

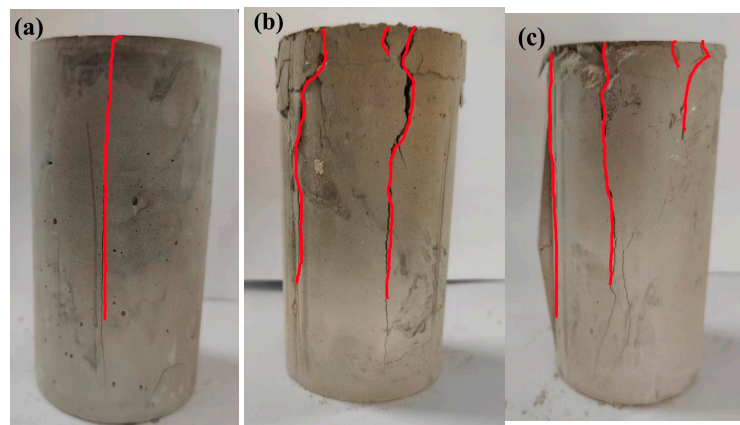


Figure 3. Compressive strength test results. (a) shear failure, (b) undergoes crush, (c) delamination failure.

3. Response Surface Methodology Analysis

3.1. Selection of Coagulants

The setting time of the RW material chosen for the experiment is 567 min. The long condensation time and the phenomenon of water secretion will lead to the formation of air leakage channels in the boreholes, which will cause the boreholes to not be sealed tightly and affect the overall pumping effect of the mine. Three kinds of coagulants were selected to study the effect of different kinds of coagulant and dosage on the setting time of the RW material. The experimental program is shown in Table 1. The experimental results are shown in Figure 4.

Table 1. Design of different kinds of coagulants dosage programs.

Coagulants Kinds	Dosage/g		
Coagulant A	2	4	6
Coagulant B	1	2	3
Coagulant C	2	4	6

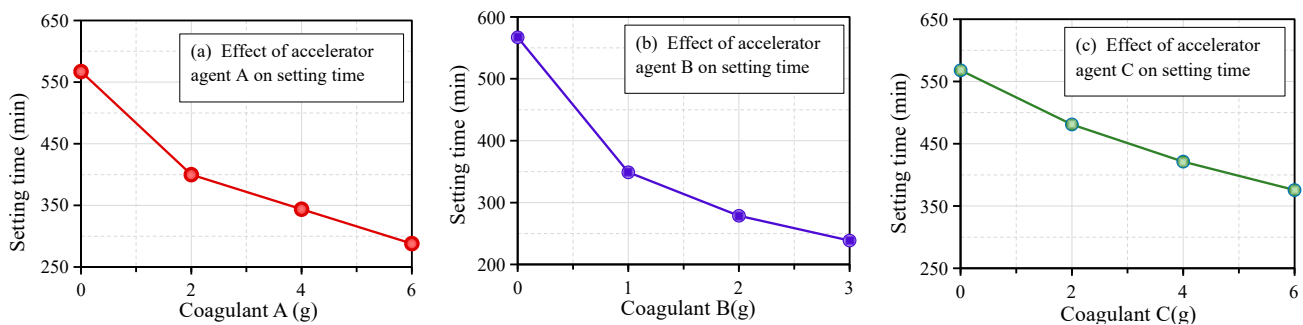


Figure 4. Effect of type and dosage of coagulants on setting time of RW materials.

The experimental results show that the setting time of the RW material is 567 min without adding coagulants. From Figure 4a, the dosage of coagulant A is 2 g, and the setting time of the RW material is 400 min, which is 29.45% shorter than that without coagulants. In addition, the setting time of RW materials are shortened by 60.85% and 48.85% at the dosage of coagulant A are 4 g and 6 g, respectively, indicating that when 4 g of coagulant A is added, the setting time of the RW material achieves the maximum reduction.

In accordance with Figure 4b, the dosage of coagulant B is 1 g, the setting time of the RW material is reduced by 38.27% compared with that without coagulants. However, the setting time of the RW material is decreased by 50.62% when the dosage of coagulant B is 2 g. When the dosage of coagulant B is 3 g, the setting time of the RW material is reduced

by 57.67%. This shows that when the dosage of coagulant B is 3 g, the setting time of the RW material achieves maximum reduction.

As demonstrated in Figure 4c, when the dosage of coagulant C is 2 g, the setting time is shortened by 15.34%. The setting times of the RW materials are shortened by 25.93% and 33.86% when the dosage of coagulant C are 4 g and 6 g, respectively. Therefore, the shortening of the setting time of RW material is greatest when the dosage of coagulant C is 6 g.

As can be seen from Figure 4, the addition of coagulants is able to reduce the setting time of the RW material. Coagulants A and B show strong hydration promoting ability, which can greatly shorten the coagulation time of the RW material. Therefore, the combination of coagulants A and B, supplemented with a suspending agent, was selected for the study of accelerated coagulation modification of the RW material.

3.2. Experimental Response Surface Study

3.2.1. Experimental Design and Results

RSM is a design methodology for establishing the accuracy of mathematical modeling to achieve optimum performance and economy [30,31]. This method is used to investigate the relationship between water–cement ratio (X_1), coagulant A (X_2), coagulant B (X_3), and suspending agent dosage (X_4) interactions with the response targets of setting time (Y_1), water secretion rate (Y_2), and compressive strength (Y_3). The response model of the surfaces was designed using Design-Expert software. Central composite response surface analysis was applied to implement the program design, and a total of 29 groups were designed. The design of test factors and levels is shown in Table 2, and the detailed mix ratios and test results are shown in Table 3.

Table 2. Coding levels of factors in the text design.

Factors	Variables	Level		
		−1	0	1
Water–cement ratio	X_1	0.8	1.0	1.2
Coagulant A	X_2	2	4	6
Coagulant B	X_3	1	2	3
Suspending agent	X_4	5	10	15

Table 3. Detailed mix ratio and test results of RW.

Group	Level				Results		
	X_1	X_2	X_3	X_4	Y_1/min	$Y_2/\%$	Y_3/MPa
1	0	0	0	0	360	0.98	6.52
2	0	1	1	0	408	1.03	7.95
3	0	0	0	0	304	1.02	7.74
4	1	0	0	−1	240	0.61	11.41
5	0	1	0	1	300	1.06	8.56
6	1	1	0	0	276	0.89	7.3
7	−1	0	0	−1	516	2.35	5.45
8	−1	1	0	0	400	1.08	6.52
9	0	0	−1	−1	304	1.02	7.74
10	0	−1	1	0	272	0.93	8.37
11	1	0	−1	0	304	1.02	7.74
12	0	−1	0	−1	492	1.96	5.1
13	0	0	1	1	296	0.96	8.55
14	0	0	1	−1	480	1.77	5.91
15	0	0	0	0	240	0.61	11.41
16	1	−1	0	0	208	0.55	11.82
17	0	1	−1	0	420	1.13	7.92
18	−1	0	1	0	296	0.95	6.11
19	1	0	1	0	516	2.35	5.45
20	1	0	0	1	400	1.08	6.52
21	0	0	0	0	276	0.89	7.3
22	0	0	−1	1	280	0.99	7.25
23	0	0	0	0	304	1.02	7.74
24	0	1	0	−1	500	1.83	4.47
25	−1	0	0	1	404	1.07	8.96
26	−1	0	−1	0	176	0.44	11.15
27	0	−1	0	1	472	1.42	4.89
28	−1	−1	0	0	484	1.65	5.1
29	0	−1	−1	0	304	1.02	7.74

3.2.2. Analysis of Regression Model

The data in Table 3 were used to fit a polynomial model that represents Y_1 , Y_2 , and Y_3 as a function of X_1 , X_2 , X_3 , and X_4 . On the basis of the results of RSM, the response equation can be expressed as:

$$Y_1 = 304 + 130.67X_1 - 26.33X_2 - 58.33X_3 - 6.67X_4 + 8X_1X_2 + 11X_1X_3 + X_1X_4 + 9X_2X_4 + 2X_3X_4 + 34.17X_1^2 + 23.67X_2^2 + 24.67X_3^2 + 17.17X_4^2 \tag{2}$$

$$Y_2 = 1.02 + 0.64X_1 - 0.013X_2 - 0.144X_3 - 0.068X_4 - 0.01X_1X_2 - 0.17X_1X_3 - 0.05X_1X_4 - 0.003X_2X_3 + 0.02X_2X_4 + 0.09X_3X_4 + 0.18X_1^2 - 0.009X_2^2 - 0.007X_3^2 + 0.008X_4^2 \tag{3}$$

$$Y_3 = 7.74 - 3.1X_1 + 0.913X_2 - 0.313X_3 + 0.006X_4 + 0.07X_1X_4 - 0.025X_1X_3 + 0.058X_2X_3 - 0.003X_2X_4 + 0.005X_3X_4 + 0.589X_1^2 - 0.111X_2^2 - 0.047X_3^2 - 0.085X_4^2 \tag{4}$$

Analysis of variance (ANOVA) determined that the quadratic regression Equations (2)–(4) could explain the experimental data at a 95% confidence level [32]. The ANOVA of the quadratic model for setting time, water secretion rate, and compressive strength is shown in Table 4. P is the significance value, and F is the ratio of the mean squared error to its error, which is an important indicator of ANOVA. $0.01 < P < 0.05$ indicates significant, $P < 0.01$ indicates highly significant, and $P > 0.05$ indicates not significant [33]. R^2 reflects the degree of difference between the response and actual value. A large R^2 corresponds to better model correlation [34,35]. The R^2 of the models Y_1 , Y_2 , and Y_3 were 97.77%, 97.39%, and 99.63%, respectively, with a CV < 10%, indicating that the experimental results had high credibility and accuracy. This model can be used to optimize the setting time, water secretion rate, and compressive strength of the RW material.

Table 4. Response surface ANOVA results.

Data Sources	Degrees of Freedom	Setting Time		Water Secretion Rate		Compressive Strength	
		F	P	F	P	F	P
Model	14	30.8	<0.0001	37.27	<0.0001	268.78	<0.0001
X_1	1	335.88	<0.0001	458.67	<0.0001	3353.07	<0.0001
X_2	1	13.64	0.0006	0.2022	0.6598	292	<0.0001
X_3	1	0.8743	<0.0001	5.18	0.0003	34.18	<0.0001
X_4	1	66.94	0.2875	23.64	0.0390	0.0119	0.9146
X_1X_2	1	7.95	0.0155	0.0379	0.8484	15.72	0.0019
X_1X_3	1	5.44	0.0378	11.28	0.0047	13.31	0.0033
X_1X_4	1	0.0066	0.9366	6.05	0.0324	1.05	0.3254
X_2X_3	1	6.38	0.0281	1.47	0.2856	5.26	0.0407
X_2X_4	1	3.95	0.0755	0.0976	0.7593	1.12	0.3102
X_3X_4	1	0.0262	0.8737	8.93	0.0245	0.0029	0.9577
X_1^2	1	8.44	0.0115	19.55	0.0006	65.68	<0.0001
X_2^2	1	3.32	0.0899	0.0517	0.8235	2.32	0.1496
X_3^2	1	6.71	0.0448	0.0385	0.8472	1.35	0.2641
X_4^2	1	1.33	0.2688	0.0309	0.8631	0.4195	0.5277
Lack of Fit	10	1	0.5464	9.77	0.0732	11.04	0.0865
		$R^2 = 0.9777$		$R^2 = 0.9739$		$R^2 = 0.9963$	
		$R_{adj}^2 = 0.9533$		$R_{adj}^2 = 0.9477$		$R_{adj}^2 = 0.9926$	
		CV% = 6.05		CV% = 9.43		CV% = 2.35	

3.2.3. Analysis of Response Surface

RSM is a statistical experimental design used to establish a continuous variable surface model, evaluate the influencing factors and their interactions of an indicator, determine the optimal level range, and require a relatively small number of experimental groups, which can save manpower and resources [36,37]. Therefore, this method has been successfully and widely applied. The significant terms ($P < 0.05$) were used to propose models for each response, without damaging the model hierarchy. These models were then tested

for adequacy and fitness by analysis of variance (ANOVA). The response surface plots were generated to visualize the combined effect of two variables on a particular response. Three-dimensional diagrams based on two independent variables were constructed, as shown in Figures 5–7 to investigate the effects of the water–cement ratio, coagulant A, coagulant B, and suspending agent interaction on setting time, water secretion rate, and concrete compressive strength of the RW material.

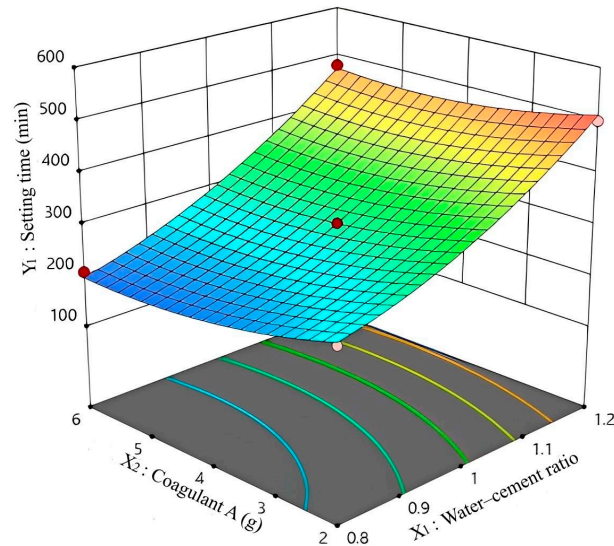


Figure 5. Factor interactions on slurry setting time.

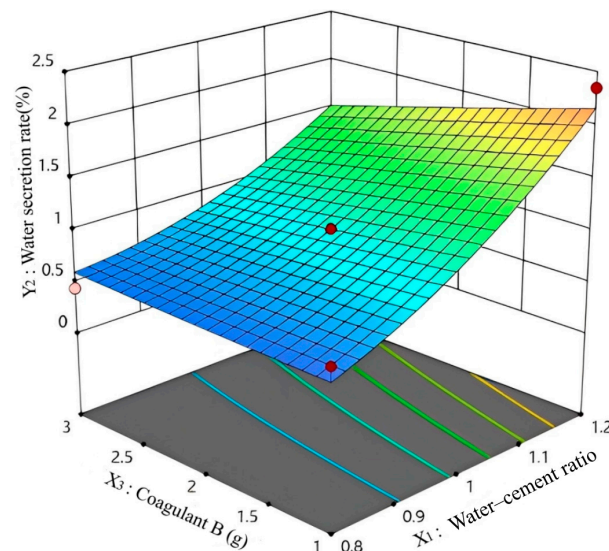


Figure 6. Factor interaction on slurry water secretion rate.

(1) Effect of interaction factors on setting time

The model ANOVA results in Table 4 show that the correlation coefficients $R^2 = 0.9777$ and $R_{adj}^2 = 0.9533$ are close to 1, indicating a strong correlation between actual and prediction. The coefficient of variation $CV = 6.05\%$ ($<10\%$) indicates that the model has a high level of confidence, explaining 97.77% of the variation in response values, and only 2.23% of the total variation could not be used in the model explanation, making the model an appropriate choice. X_1 ($P < 0.0001$), X_2 ($P = 0.0006$), and X_3 ($P < 0.0001$) are highly significant. X_1X_2 , X_1X_3 , X_2X_3 , X_1^2 , X_3^2 , and X_4^2 are significant. The degree of influence of the primary factors on the setting time (Y_1) is $X_1 > X_4 > X_2 > X_3$, indicating that the water–cement ratio has the greatest influence on the setting time. The degree of influence

of interaction on the condensation time is $X_1X_2 > X_2X_3 > X_1X_3 > X_2X_4 > X_3X_4 > X_1X_4$, thus indicating that the interaction effect of the water–cement ratio and coagulant A on setting time is the most significant.

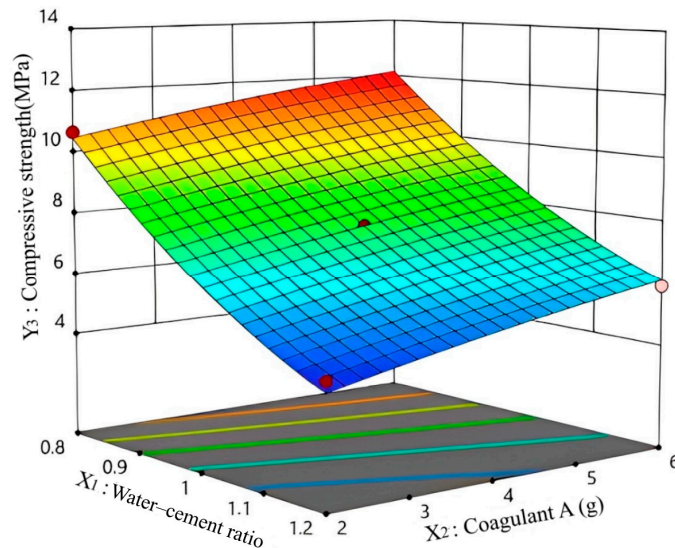


Figure 7. Factor interactions on compressive strength.

Figure 5 shows that the setting time of the RW material decreases with the increase in coagulant A when the water–cement ratio is a fixed value. When the amount of coagulant A is fixed, the setting time of the RW material is significantly prolonged with the increase in the water–cement ratio. Compared with changing coagulant A, increasing the water–cement ratio has a more significant effect on setting time. The main reason for this condition is that when the coagulant A is fixed, in the case of low water–cement ratio, the spacing of cement clinker particles in the slurry after mixing is smaller, and more cement clinker particles are present in the unit volume. Therefore, the hydration reaction of slurry per unit volume and unit time is slower, and the number of hydration products is less, thereby resulting in a longer time needed for the hydration products to lap and penetrate, and the slower formation of the skeleton structure, resulting in a longer setting time.

(2) Effect of interacting factors on water secretion rate

The results of the response surface ANOVA in Table 4 ($P < 0.0001$, $F = 37.27$) show a significant relationship between Y_2 and interacting factors. The lack of fit is not significant ($F = 9.77$, $P = 0.0732$), indicating that the regression model was a good fit. The coefficient of determination $R^2 = 0.9739$ suggests a strong correlation between the actual and predicted values. Furthermore, the coefficient of variation $CV = 9.43\%$ ($< 10\%$) is reasonable and the model can explain 97.39% of the variation in response values, thereby implying that the model is chosen appropriately. The effect of X_1 ($P < 0.0001$), X_3 ($P = 0.0003$), and X_1X_3 ($P = 0.0047$) on Y_2 is highly significant. The effect of X_4 , X_1X_4 , and X_3X_4 on water secretion rate is significant. The degree of influence of the primary term on the urinary rate is $X_1 > X_4 > X_3 > X_2$, indicating that the water–cement ratio has the greatest effect on the water secretion rate. The degree of influence of the secondary term on the water secretion rate is $X_1X_3 > X_3X_4 > X_1X_4 > X_2X_3 > X_2X_4 > X_1X_2$, indicating that the interaction of X_1 and X_2 had the greatest influence on the water secretion rate.

As can be seen from Figure 6, when the water–cement ratio is a fixed value, the water secretion rate with the increase in coagulant B. When the amount of coagulant B is fixed, the water secretion rate increases significantly with the increase in the water–cement ratio, especially in the case of coagulant dosage is 1 g, and the degree of increase in the water secretion rate is greater. This condition occurred mainly because coagulant B is unchanged and has a low water–cement ratio. Moreover, uniform slurry cement clinker particles in

the spacing are smaller, with more cement clinker particles per unit volume. In the unit time per unit volume of slurry hydration reaction is faster, hydration products between the rapid formation of a skeletal structure, locking the water to reduce the amount of free water, thus reducing the water secretion rate. Similarly, a large water–cement ratio corresponds to fewer cement clinker particles per unit volume. As a result, hydration products lap require a longer time, and the formation of the skeleton structure is slower. Moreover, a large volume of free water is present in the slurry system, leading to an increase in water secretion rate. Coagulant B has an inhibitory effect on the slurry water secretion rate by accelerating the formation of the skeleton structure, thereby shortening the slurry setting time, which, in turn, reduces the free water content in the slurry system to reduce the water secretion rate.

(3) Effect of interaction factors on compressive strength

The ANOVA results in Table 4 show that the correlation coefficient $R^2 = 0.9963$ and $R_{adj}^2 = 0.9926$ are close to 1 in the response surface model, indicating that the designed model has rationality and consistency. Moreover, $F = 268.71$, $P < 0.0001$, and the coefficient of variation $CV = 2.35\%$ ($<10\%$), indicating that this response surface model has a significant effect on the experimental results and can explain 99.63% of the variation in response values. Thus, the model is appropriately selected. X_1 , X_2 , X_3 , X_1X_2 , and X_1X_3 are highly significant for the compressive strength (Y_2), and X_2X_3 is significant for the compressive strength. The degree of influence of the primary term on the compressive strength is $X_1 > X_2 > X_3 > X_4$, indicating that the water–cement ratio has the greatest effect on the compressive strength. The degree of influence of the quadratic term on the compressive strength is $X_1X_2 > X_1X_3 > X_2X_3 > X_2X_4 > X_1X_4 > X_3X_4$, indicating that the interaction of the water–cement ratio and coagulant A has the greatest effect on the compressive strength.

Figure 7 shows that for a fixed water–cement ratio, the compressive strength increases with increasing coagulant A. For a constant volume of coagulants, the compressive strength decreases with the increase in water–cement ratio mainly because in slurries, the amount of water that can react chemically with the cement component is limited. When the water–cement ratio is high, the slurry has excess water, although the slurry can retain the excess water after setting to prevent water secretion. However, with the increase in time, the excess water will cause the solidified body microstructure to have more voids and be less dense, thus reducing compressive strength. The hydration products of coagulant A are mainly calcium sulfoaluminate hydrates, hydrated calcium silicate gel, calcium hydroxide crystals, and aluminum gel. Thus, the amount of AFt produced by the hydration reaction in the slurry is higher than that produced in the ordinary silicate slurry. As a result, the grouted consolidation is less porous and denser, thus having improved strength.

Table 4 and Figures 5–7 show that increasing the water–cement ratio can increase the setting time and the water secretion rate of the RW material, but weaken the compressive strength of the solids. The X_1X_2 interaction has the greatest effect on the setting time and compressive strength of the RW material. The X_1X_3 interaction has the greatest effect on the water secretion rate of the grouting material.

4. Microscopic Interface Analysis of Slurry–Coal Solids

4.1. Microscopic Morphology Analysis of Grouting Materials

SEM can visually and accurately predict the three-dimensional structure of the surface of the sample under test [38]. In the present research, the microstructural characteristics of the concretion after grouting of broken coal samples are investigated using SEM, as shown in Figure 8.

The figure depicts that the grouting materials contain needle-like AFt, six-sheeted CH crystals, and C-S-H gels, which are interweaved to form a spatial network-like structure. The density of the RW material is higher, as shown in Figure 8a, because the coagulant added to the RW material can increase the number of needle-like AFt in the hydration products and fill the pore structure of the cementitious material. The hydration products form a skeleton structure between them, and the generated hydrated C-S-H gel overlaps to form

a relatively dense network structure, thus causing the slurry to settle quickly, increasing the structural densification, and improving the strength of the solid. The microstructure in Figure 8b shows that the AFt crystals of PC material are loosely connected, and the resulting network structure has larger fractures, resulting in higher permeability compared with the RW.

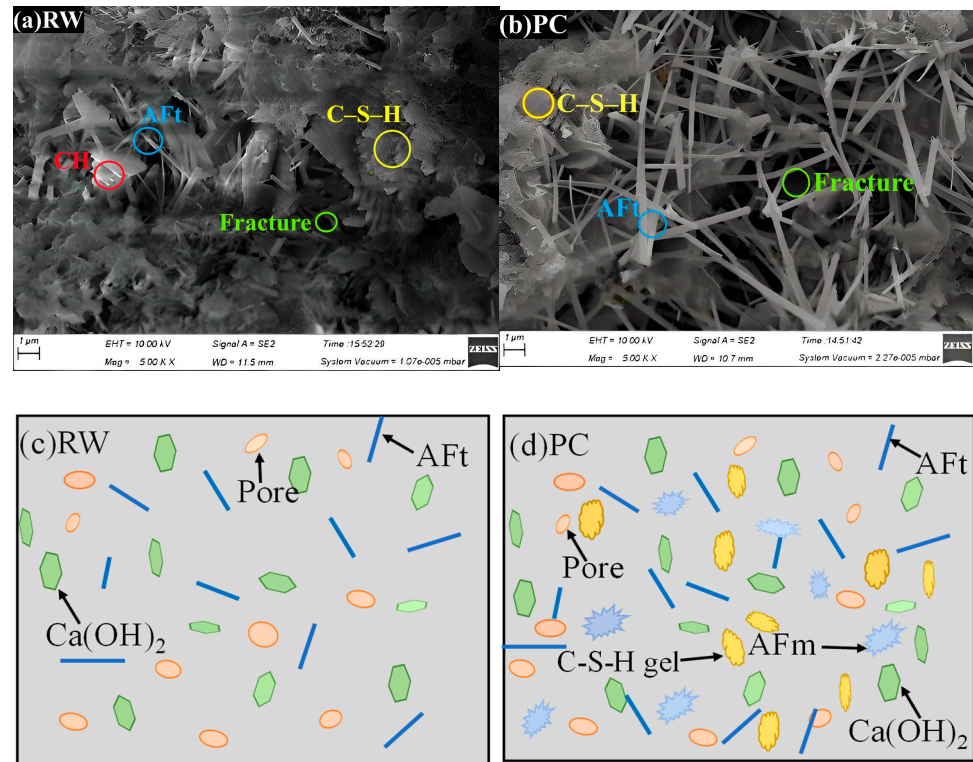


Figure 8. Hydration products of different grouting materials. (a) microstructure of RW material, (b) microstructure of PC material, (c) schematic diagram of the microscopic hydration process of RW material, (d) schematic diagram of the microscopic hydration process of PC material.

4.2. Microscopic Morphology Analysis of Slurry–Coal Solids

The interfacial transition zone (ITZ) is an important component of the concretion, characterized by low strength and low modulus of elasticity, which affects compressive strength and permeability [39,40]. The transition zone at the grouting materials and injected coal interface exhibits differences because of the difference in the PC and RW grouting materials. In this study, we investigated the microscopic morphology of the slurry–coal transition zone in different concretes. The SEM results are presented in Figure 9.

As shown in Figure 9a,b, the fracture at the interface of the grouting materials and injected coal of the RW material is smaller than that of the PC material at 5000× magnification, indicating that the bonding between the RW material and the coal is better. This condition can be attributed to the presence of a high concentration of hydration products filled within the RW material and the coal. These products interweave to form a compact network structure that can endure some stress and absorb energy when subjected to an external load. As a result, the strength of the ITZ of the RW material is improved. In contrast, the ITZ of the PC has fewer hydration products, resulting in a looser skeletal structure and insufficient bonding strength, and is, thus, prone to misalignment and separation under external loading.

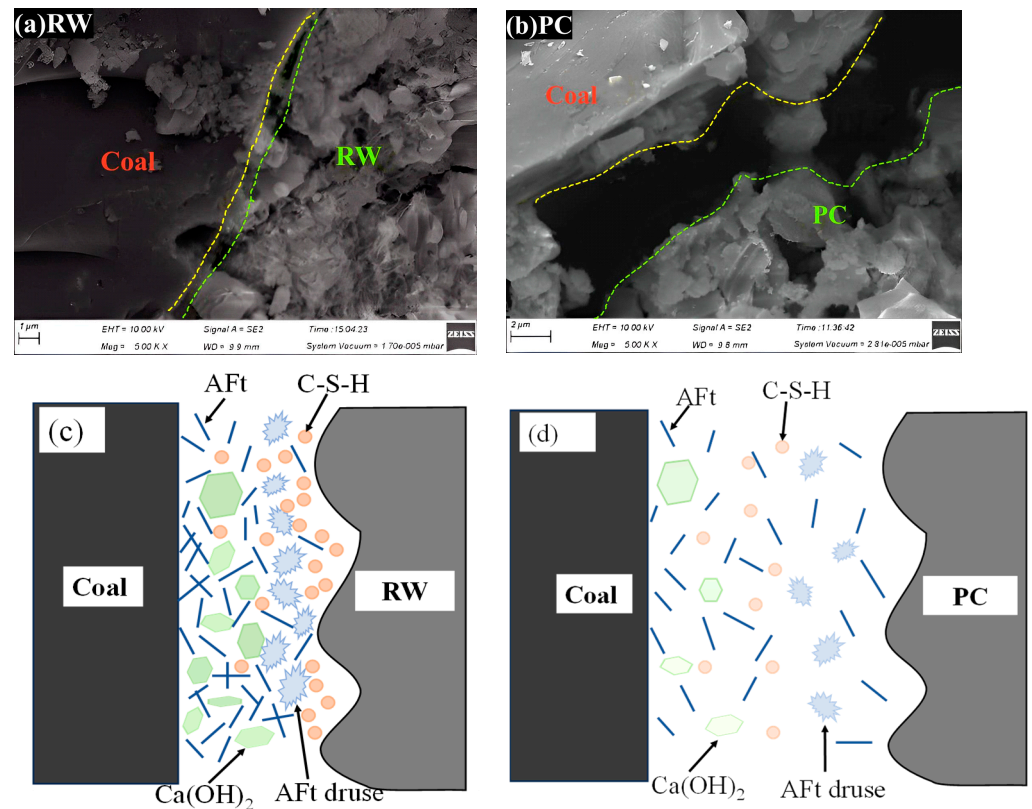


Figure 9. ITZ microstructure of different concretion samples. (a) microscopic morphology of the slurry—coal transition zone of RW material, (b) microscopic morphology of the slurry—coal transition zone of PC material, (c) schematic diagram of hydration process in slurry—coal transition zone of RW material, (d) schematic diagram of hydration process in slurry—coal transition zone of PC material.

Figure 9c,d present the microscopic cementation model of the RW and PC materials. Ordinary cement has a low hydration degree, which later leads to shrinkage boreholes. As a result, short columnar AFt and CH gel hydration products are formed. The C_4A_3S' minerals supplied by the coagulants experience additional hydration with the mineral particles in the cement, forming fine-needle AFt. The increased number of crystals results in the densification of pores within the pristine cement particles. The microscopic properties of the RW grouting materials have a significant effect on their macroscopic mechanical properties. This effect is due to the rapid early-stage hydration of the C_3A , C_3S , and C_2S minerals in cement, forming the C-S-H gel and CH crystals, and the reaction of the C_4A_3S' minerals with calcium sulfate to form AFt and CH gels, accelerating the early hydration rate. The hydration products, AFt crystals, C-S-H gels, and lamellar CH crystals interact with each other. The particles depend on van der Waals forces and chemical bonding to provide cured paste properties, including microexpansion and mechanical strength.

5. Conclusions

(1) The effect of different coagulant additives on the RW material was investigated using one-factor analysis. The experimental results demonstrate that coagulants A and B exhibit strong hydration-promoting abilities, which significantly shorten the setting time of the RW material. When the coagulants A is 4 g and coagulants B is 2 g, the setting time of RW material reduced by 60.85% and 50.62%, respectively. Therefore, coagulants A and B were selected for the compounding process and, then, supplemented with suspending agents to study the coagulant modification of the RW material. The water–cement ratio and setting time should be strictly controlled when adding the coagulant additives to avoid affecting the engineering practice effect.

(2) The RSM was used to investigate the effect of each factor on the setting time, water secretion rate, and compressive strength of the RW material. A quadratic regression response model was fitted to indicate the influence of the interaction of each factor. The ANOVA results demonstrated that all models were statistically significant with P values less than 0.0001 and the model precision was high, effectively reflecting the degree of influence. All the correlation coefficients R^2 of each response model were greater than 0.97 through variance analysis, indicating a high correlation between the actual and prediction results. The water–cement ratio had the most significant effect among all factors on setting time, water secretion rate, and compressive strength of the RW material. Coagulant B and water–cement ratio interaction had the second-greatest effect.

(3) The microstructure of the RW and PC materials was analyzed by SEM. The SEM microstructure of the coagulant-doped RW material showed an increase in the number of needle-like AFt crystals, which filled the internal pore structure of the material, and a cross-linked skeletal structure was formed between the hydration products, which was denser than the network structure of the PC material. The slurry–coal interface of the RW had no fractures, which showed that its sealing effect was superior to that of the PC grouting material.

Author Contributions: X.L.: conceptualization and investigation. G.H.: funding and software. Y.W.: investigation and writing—original draft. J.X.: conceptualization, methodology, and funding. J.D.: data curation and supervision. B.Y.: investigation and validation. M.Z.: investigation and methodology. T.L.: writing—review. B.L.: editing, funding and supervision. All authors have read and agreed to the published version of the manuscript.

Funding: The authors sincerely thank the following agents for their financial supports: the National Natural Science Foundation of China (grant no. 52274190), the Sponsored by Program for Science & Technology Innovation Talents in Universities of Henan Province (no. 23HASTIT008), and the Henan Provincial Science and Technology Research Project (no. 222102320086).

Data Availability Statement: The data applied to support the results in this study are available from the corresponding author upon request.

Conflicts of Interest: The authors declare no conflict of interest.

References

1. Asif, M.; Wang, L.; Wang, R.; Wang, H.; Hazlett, R. Mechanisms in CO₂-enhanced coalbed methane recovery process. *Adv. Geo-Energy Res.* **2022**, *6*, 531–534. [[CrossRef](#)]
2. Andrews-Speed, P.; Xu, X.; Jie, D.; Chen, S.; Zia, M. Deficiencies in China’s innovation systems for coal-bed methane development: Comparison with the USA. *J. Sci. Technol. Policy Manag.* **2023**, *14*, 511–528. [[CrossRef](#)]
3. Wu, A.; Ruan, Z.; Raimund, B.; Yin, S.; Wang, J.; Wang, Y. Optimization of flocculation and settling parameters of tailings slurry by response surface methodology. *Miner. Eng.* **2020**, *156*, 106488. [[CrossRef](#)]
4. Gao, Q.; Yang, X.; Wen, Z.; Chen, D.; He, J. Optimization of proportioning of mixed aggregate filling slurry based on BBD response surface methodology. *J. Hunan Univ. Nat. Sci.* **2019**, *46*, 6.
5. Wang, H.; Fan, C.; Li, J.; Wu, Y.; Xing, S.; Wang, W. A Field Study of Coal Fire Areas Re-Burning Behavior Assessment and Related Carbon Emissions. *Fire* **2022**, *5*, 186. [[CrossRef](#)]
6. Bosikov, I.; Martyushev, N.; Klyuev, R.; Savchenko, I.; Kukartsev, V.; Tynchenko, Y. Modeling and complex analysis of the topology parameters of ventilation networks when ensuring fire safety while developing coal and gas deposits. *Fire* **2023**, *6*, 95. [[CrossRef](#)]
7. Silva, D.; Nuzzo, I.; Nigro, E.; Occhiuzzi, A. Intumescent coatings for fire resistance of steel structures: Current approaches for qualification and design. *Coatings* **2022**, *12*, 696. [[CrossRef](#)]
8. Zhang, J.; Li, G.; Meng, Z.; Zhang, Y.; Liu, L.; Li, D.; Xu, Y. Key technology of surface extraction for coalbed methane wells crossing goaf. *J. China Coal Soc.* **2020**, *45*, 2552–2561.
9. Joshi, D.; Prajapati, P.; Sharma, P.; Sharma, A. Past, present and future of coal bed methane (CBM): A review with special focus on the Indian scenario. *Int. J. Coal Prep. Util.* **2023**, *43*, 377–402. [[CrossRef](#)]
10. Zhu, C.; Zhang, J.; Li, M.; He, Z.; Wang, Y.; Lan, Y. Effect mechanism of strata breakage evolution on stope deformation in extra-thick coal seams. *Alex. Eng. J.* **2022**, *61*, 6. [[CrossRef](#)]
11. Kędzior, S.; Teper, L. Coal Properties and Coalbed Methane Potential in the Southern Part of the Upper Silesian Coal Basin, Poland. *Energies* **2023**, *16*, 3219. [[CrossRef](#)]
12. Wang, H.; Li, B.; Wang, Y.; Li, S.; Zhang, G.; Yang, D. Key technology and bottlenecks of multi-energy complementary DC microgrid for residual coalbed methane in abandoned mine. *J. China Coal Soc.* **2023**, *48*, 1798–1813.

13. Jia, Q.; Liu, D.; Cai, Y. Research progress on wells interference in coalbed methane mining. *J. China Coal Soc.* **2020**, *45*, 882–893.
14. Wang, Z.; Zhou, Y.; Sun, Y.; Wang, Y. Novel gas extraction borehole grouting sealing method and sealing mechanism. *J. China Coal Soc.* **2015**, *40*, 588–595.
15. Zhang, J.; Liu, Y.; Ren, P. A fully multifield coupling model of gas extraction and air leakage for in-seam borehole. *Energy Rep.* **2021**, *7*, 1293–1305. [[CrossRef](#)]
16. Wang, H.; Wang, E.; Li, Z.; Wang, X.; Zhang, Q.; Li, B. Ali Muhammad. Study on sealing effect of pre-drainage gas borehole in coal seam based on air-gas mixed flow coupling model. *Process Saf. Environ. Prot.* **2020**, *136*, 15–27. [[CrossRef](#)]
17. Si, L.; Shi, W.; Wei, J.; Liui, Y.; Yao, B. Self-healing characteristics of fracture in sealing materials based on self-healing effect. *J. China Coal Soc.* **2023**, 1–14. [[CrossRef](#)]
18. Xia, T.; Zhou, F.; Liu, J.; Hu, S.; Liu, Y. A fully coupled coal deformation and compositional flow model for the control of the pre-mining coal seam gas extraction. *Int. J. Rock Mech. Min. Sci.* **2014**, *72*, 138–148. [[CrossRef](#)]
19. Chen, X.; Zhou, T.; Zhou, J.; Ma, L.; Liu, Q.; Xu, X. Study on the flame retardant property of reactive halogen-free organic grouting reinforcement materials for coal mines. *Min. Saf. Environ. Prot.* **2023**, *50*, 40–45.
20. Sun, W.; Guo, B.; Zhang, R. Effect of hydroxide properties of new material for sealing gas drainage boreholes. *China Saf. Sci. J.* **2016**, *26*, 98–102.
21. Zhao, Y.; Sun, Y.; Wang, Z. Mixed volume of aluminous cement affected to grouting material performances of borehole sealing for gas drainage. *Coal Sci. Technol.* **2018**, *46*, 146–152.
22. Liu, J.; Luo, Q.; Ji, X.; Wu, F.; Ma, M.; Zhang, C.; Wang, Q. Study on preparation and performance of an early strength grouting materials. *J. Saf. Sci. Technol.* **2018**, *14*, 95–99.
23. Qian, Z.; Han, B. Experimental study on water absorption performance of super absorbent resin in sealing and grouting process of gas drainage borehole. *Saf. Coal Mines* **2020**, *51*, 32–36.
24. Guan, X.; Li, X.; Zhang, H.; Yang, Z.; Li, H.; Di, H.; Zhang, L. Research and application of inorganic composite grouting reinforcement materials in deep weak rock. *Coal Sci. Technol.* **2023**, *51*, 1–11.
25. Liu, J.; Feng, H.; Zhang, Y.; Zheng, K. Performance Investigation of Geopolymer Grouting Material with Varied Mix Proportions. *Sustainability* **2022**, *14*, 13046. [[CrossRef](#)]
26. Zhang, J.; Wang, X.; Jin, B.; Zhang, X.; Li, Z.; Guan, X. Effect of superplasticizers on hydration kinetics of ultrafine sulfoaluminate cement-based grouting material. *Thermochim. Acta* **2021**, *703*, 178988. [[CrossRef](#)]
27. Ruan, W.; Zhang, Z.; Cai, M.; She, Y.; Liu, J.; Guo, W.; Ma, X.; Liao, J.; He, X. Comparative study of the effects of magnesium aluminum silicate and bentonite clay on the properties of magnesium phosphate cement-based grouting material. *Constr. Build. Mater.* **2023**, *401*, 132852. [[CrossRef](#)]
28. Choudhury, S.; Jena, T. Influence of surfactant on foam generation and stabilization in cement slurry. *Mater. Today Proc.* **2023**. [[CrossRef](#)]
29. Mahmood, W.; Mohammed, A.; Asteris, P.; Kurda, R.; Armaghani, D. Modeling flexural and compressive strengths behaviour of cement-grouted sands modified with water reducer polymer. *Appl. Sci.* **2022**, *12*, 1016. [[CrossRef](#)]
30. Pereira, L.; Milan, T.; Tapia-Blácido, D. Using Response Surface Methodology (RSM) to optimize 2G bioethanol production: A review. *Biomass Bioenergy* **2021**, *151*, 106166. [[CrossRef](#)]
31. Liu, Y.; Zhao, C.; Li, G.; Zhao, X.; Li, Z.; Zhang, X.; Li, Y.; Guo, J.; Guo, D. Optimized decision method of coordinated development mode of coal and coalbed methane in Jincheng mining area. *J. China Coal Soc.* **2020**, *45*, 2575–2589.
32. Liang, W.; Zhang, B.; He, W.; Yao, H. Experimental research on supercritical CO₂ enhanced coalbed methane recovery in different rank coals. *J. China Coal Soc.* **2020**, *45*, 197–203.
33. Zhang, J.; Liu, L.; Li, Q.; Peng, W.; Zhang, F.; Cao, J.; Wang, H. Development of cement-based self-stress composite grouting material for reinforcing rock mass and engineering application. *Constr. Build. Mater.* **2019**, *201*, 314–327. [[CrossRef](#)]
34. Zhang, Y.; Wang, Y.; Wu, Z.; Lu, Y.; Kang, A.; Xiao, P. Optimal design of geopolymer grouting material for semi-flexible pavement based on response surface methodology. *Constr. Build. Mater.* **2021**, *306*, 124779. [[CrossRef](#)]
35. Petruniak, M.; Rubel, V.; Chevhanova, V.; Kulakova, S. Application of grout slurries with the defecate addition for effective well cementing. *Min. Miner. Depos.* **2021**, *15*, 59–65. [[CrossRef](#)]
36. Liu, W.; Sun, Y.; Meng, X.; Qin, Y. Experimental analysis of Nano-SiO₂ modified waterborne epoxy resin on the properties and microstructure of cement-based grouting materials. *Energy* **2023**, *268*, 126669. [[CrossRef](#)]
37. Liu, J.; Li, X.; He, T. Application status and prospect of backfill mining in Chinese coal mines. *J. China Coal Soc.* **2020**, *45*, 141–150.
38. Behnia, B.; AaliAnvari, A.; Nazari, M. A study to examine the effect of grouting superfine cement slurry containing nano-silica additives by a simulator cylinder in environments with many joints and gaps. *Arab. J. Geosci.* **2021**, *14*, 1–15. [[CrossRef](#)]
39. Wei, Z.; Yang, K.; He, X.; Zhang, J.; Hu, G. Experimental study on the optimization of coal-based solid waste filling slurry ratio based on the response surface methodology. *Materials* **2022**, *15*, 5318. [[CrossRef](#)] [[PubMed](#)]
40. Basu, P.; Thomas, B.S.; Gupta, R.C.; Vinay, A. Properties of sustainable self-compacting concrete incorporating discarded sandstone slurry. *J. Clean. Prod.* **2021**, *281*, 125313. [[CrossRef](#)]

Disclaimer/Publisher's Note: The statements, opinions and data contained in all publications are solely those of the individual author(s) and contributor(s) and not of MDPI and/or the editor(s). MDPI and/or the editor(s) disclaim responsibility for any injury to people or property resulting from any ideas, methods, instructions or products referred to in the content.